Impact of turbulence on the coherent flame dynamics in a bluff-body stabilized flame

Ashwini Karmarkar[a], Ankit Tyagi[a], Santosh Hemchandra[b], Jacqueline O'Connor[a,*]

[a]*Pennsylvania State University, University Park, PA 16802, USA*
[b]*Indian Institute of Science, Bengaluru, KA 560012, India*

Abstract

Coherent flame oscillations generated by large-scale flow instabilities have been shown to significantly influence combustor performance and thermoacoustic instability. This study examines the influence of turbulence intensity on the large-scale dynamics of rod-stabilized flames. Instability in the flow field of a bluff-body stabilized flame, which is a function of mean shear in the flow field, turbulence intensity of the incoming flow, and the location of the flame with respect to the shear layer, manifests as coherent vortex shedding. However, this vortex shedding is not self-excited if the flow is globally stable, as is often the case in reacting flows. In this experiment, time-resolved, three-component velocity measurements from high-speed stereoscopic particle image velocimetry are taken at three turbulent inlet flow conditions and at three bulk flow velocities. To identify whether these instabilities occur, the velocities fields are filtered using a wavelet transform around select spectral bands and then decomposed using proper orthogonal decomposition to

---

*Corresponding author:
Email address: jxo22@psu.edu (Jacqueline O'Connor)

extract the most energetic motion in the flow; this filtering method retains any time-dependent, intermittent behavior. The results show that vortex shedding is intermittent and the degree of intermittency is dependent on the in-flow turbulence level. Although all the cases tested were determined to be globally stable, variations in the flow velocity change the structure of the flame and flow, which alters the receptivity of the flow to turbulent perturbations. As a result, the strength and regularity of vortex shedding increase with increasing turbulence level and increased receptivity, indicating that the system is a noise-forced globally-stable oscillator.

Estimated word count: 6113

1. Introduction

The response of flames to large-scale coherent fluctuations is an important consideration in the design of combustors [1], as coherent oscillations can be the driving mechanism of thermoacoustic instabilities. Large-scale flame dynamics also influence limiting phenomena such as blow-off and flashback [2]. Realistic combustion systems are also subject to high levels of turbulence that enhance fuel/air mixing and flame speed, where these turbulent fluctuations are incoherent and fluctuate at a range of scales. The goal of this work is to understand the impact of turbulence on the large-scale behavior of the flow and the resultant effect on flame dynamics.

The current experiment considers a bluff-body stabilized flame. The global instability of this flow manifests in the wake region as a result of

recirculation behind the bluff body. The coherent dynamics of reacting wake flows are a strong function of flame density ratio [3] and the degree of co-location between the density and velocity gradients [4]. These unstable flows are sensitive to acoustic perturbations that can drive vortex shedding in the shear layer, causing coherent flame wrinkling [5], which can lead to thermoacoustic instability.

One of the first-order impacts that turbulence can have on coherent oscillations is the effect of "vortex jitter". In work by Shanbhogue et al. [6], acoustically-driven vortices were tracked in a weakly turbulent bluff-body stabilized flame and their location varied at a given period of the acoustic cycle due to the effect of turbulence. This variability resulted in a loss of coherence of flame wrinkling and potential weakening of the thermoacoustic feedback cycle. This same effect was also seen in more complicated swirling flows by Karmarkar et al. [7]. It has also been shown that variation in turbulence intensity significantly alters the topology of the flame front, causing flames to transition from straight lines, to wrinkled surfaces, to cusps, as turbulence intensity increases [8].

When both coherent and turbulent fluctuations are present in a flow, there is also the potential for intermittency in the coherent dynamics. In non-reacting wakes, it has been suggested that intermittency arises due to streamwise movement of the point at which the shear layer separates, causing high-frequency oscillations that increase with Reynolds number [9]. The dynamics of reacting flows past bluff bodies are more complicated because of the stabilizing effect of gas expansion in the wake, which leads to both a change in the global stability of the flow and dissipation of vortical structures

3

due to gas expansion and increased viscosity. Emerson et al. [4] showed that intermittency in a vitiated bluff-body stabilized flame is a result of stochastic excitation when the flow conditions approach a supercritical Hopf bifurcation. Not all intermittency must arise from this source, however, as a variety of types of intermittent dynamics have been measured in the operating ranges near thermoacoustic instability [10]. Additionally, it has been shown that the overall flame shape of a bluff-body stabilized flame changes intermittently from symmetric to anti-symmetric as turbulence level is increased near blow off [11–13].

In this study, we aim to characterize the evolution of intermittent behavior with increasing in-flow turbulence. We consider the behavior of rod-stabilized flames at three different bulk flow velocities and three in-flow turbulence intensities. We filter the flow fields using wavelet transforms to preserve the time-varying behavior and reconstruct select spectral bands where intermittent coherent motion is measured. The reconstructed signal is then decomposed using proper orthogonal decomposition (POD) to identify the most energetic coherent motions in the selected spectral bands. This method, in contrast to directly using POD on the signal, allows us to observe time-varying coherent dynamics even when the coherence is weak and intermittent.

We quantify the observed intermittency by identifying the time-variation of coherent motion. Quantifying this influence is an important step towards interpreting the interactions between different scales of oscillations. The results are explained using principles from hydrodynamic stability theory in wakes by characterizing the degree of co-location between the flame and the shear layer.

2. Experiment and Methods

The experimental facility is a modified version of that used by Tyagi et al. [14] and only a brief overview is provided here. The flame is a rod-stabilized V-flame in an unconfined configuration. Upstream of the flame, the burner consists of a 30 mm x 100 mm burner exit with a 100 mm long, 3.18 mm diameter rod that runs along the center axis of the burner, as shown in Fig. 1. The burner contains the inlet for the premixed reactants (natural gas and air), two ceramic honeycomb flow-straighteners, and perforated plates for turbulence generation. The turbulence generation plates have a staggered hole pattern with 3.2 mm hole diameters and a 40% open area. Three combinations of perforated plates are used: two plates located 10 mm and 30 mm upstream of the burner exit for high in-flow turbulence intensity (18%), one plate located 10 mm upstream of the burner exit for mid-level in-flow turbulence intensity (14%), and no perforated plates for low in-flow turbulence intensity (6%). The test matrix used in this study is shown in Table 1. The bulk flow velocity is denoted by U, the turbulence intensity is denoted by u', and the laminar flame speed (calculated using Chemkin and GRIMech 3.0) is denoted by S_L. The turbulence intensity is calculated using three components of velocity from the high-speed PIV along the burner centerline without the rod present so that only the turbulence effects from the plates are captured in this metric. All conditions are run with stoichiometric fuel/air mixtures and room-temperature air inlet at ambient pressure.

Stereoscopic particle image velocimetry (PIV) is performed at 10 kHz with a dual cavity, Nd:YAG laser (Quantronix Hawk Duo) operating at 532 nm in forward-forward scatter mode. A 50 mm tall laser sheet is created
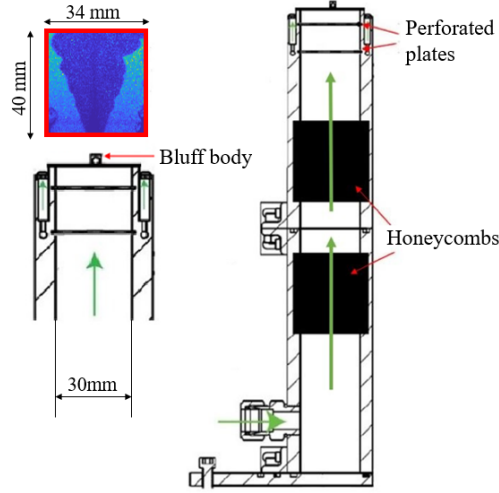
Figure 1: Burner configuration with area of analysis indicated by the red square

using a combination of mirrors and three cylindrical lenses; the angle between the laser sheet plane and each camera sensor (Photron FASTCAM SA5) is about 25 degrees. Each camera is equipped with a 100 mm f/2.8 lens (Tokina Macro) and a Nikon tele-converter to allow for a safe stand-off distance between the sensor and the burners. A 32 mm x 53 mm field of view is obtained through this setup and images are collected at 10 kHz in double frame mode with a pulse separation of 14 μs. Aluminum oxide particles of diameters 0.5-2.0 μm are used for seeding the flow field. To reduce flame luminosity, near-infrared filters (Schneider Kreuznach IR MTD) and laser line filters (Edmund Optics TECHSPEC 532 nm CWL) are used on each camera.

LaVision's DaVis 8.3 is used to perform vector calculations from Mie scattering images in the region shown by the red box in Fig. 1. These calculations include a multi-pass algorithm with varying window sizes ranging from 64 x 64 to 16 x 16 and a 50% overlap. This results in a vector spacing

Case	U (m/s)	$u'(m/s)$	u'/U	u'/S_L
High	5	0.9	18%	2.25
Turbulence	10	1.8		4.5
	15	2.7		6.75
Mid	5	0.65	14%	1.62
Turbulence	10	1.36		3.4
Low	5	0.32	6%	0.8
Turbulence	10	0.59		1.47
	15	0.87		2.17

Table 1: Test Matrix

of 0.48 mm/vector. A universal outlier detection scheme, with a 3x median filter, is used for post-processing of the vector fields. Maximum uncertainties in instantaneous velocities range from 0.6 m/s in the low-velocity case to 1.5 m/s in the high-velocity case, or 10%, using the uncertainty calculation feature in DaVis. A total of 5000 vector fields are obtained for each condition.

The Mie-scattering images are also used to identify the flame location. The process for binarization and edge detection for Mie-scattering images is as follows: (i) images are Gaussian filtered for blurring sharp gradients due to noise, (ii) median filtering with a window size of 10 pixels x 10 pixels is applied to remove the effect of salt and pepper noise due to scattering from aluminum oxide particles, (iii) smoothing operation is performed using bilateral filtering, (iv) Otsu's method is applied on the smoothed image from step (iii) and multi-level thresholding is used to account for the spatial variation in signal intensity, and (v) the minimum threshold value is used to binarize

the processed image into a value of 0 for the reactants and 1 in the products. These binarized images are used to calculate the time-averaged progress variable contour, $\bar{c}$. In this calculation, all binarized images are averaged and the $\bar{c} = 0.5$ contour is used as an indication of the time-averaged flame location. More in-depth discussion of these processes is provided in the supplementary material.

3. Results

The study conducted by Emerson et al. [4] proposed that the intermittency observed in coherent flame dynamics at turbulent conditions is due to parametric noise associated with random fluctuations in the offset of the flame location and shear layer, which can lead to a stochastic modulation of the global mode growth rate. In particular, studies show that the alignment between the shear layer and the flame can alter not only the global stability of the flow, but also the receptivity of the flow to incoming perturbation. Receptivity of a hydrodynamic instability mode is defined as the sensitivity of the mode response to external perturbation. Giannetti and Luchini [15] identified regions of the flow that are receptive to different kinds of forcing in two-dimensional, laminar wakes of cylindrical bluff bodies. They showed that highest receptivity is located near the wake of the cylinder.

Based on these previous results, we hypothesize that a globally-stable reacting wake can be driven by high-intensity turbulence such that coherent wake oscillations occur. Further, we posit that the receptivity of this wake mode to incident perturbations is a function of the offset between the shear layer and the flame. Since the density ratio of the flame in this study is

8

constant and high, the flame/shear offset is the critical stability parameter in this experiment. The noise-driven wake oscillation should arise intermittently as the incident perturbations are turbulent, rather than periodic, which we show using a new wavelet-filtered POD.

3.1. Time-averaged flow profiles

Figure 2 shows streamlines and the time-averaged vorticity for the two extreme turbulence intensity (6% and 18%) and bulk flow velocity (5 and 15 m/s) conditions; the $x = 0$ mm position in the images indicates the centerline of the bluff-body, shown in the inset of Fig. 1. At higher velocities, the mean shear magnitude increases in the two shear layers that separate from the bluff body. Increasing the in-flow turbulence intensity also increases this mean shear. The $\bar{c} = 0.5$ time-averaged progress variable contour is shown in red on each of the plots, where products are located in the center of the contour and reactants are located outside, given the flame configuration. The $\bar{c} = 0.2$ and $\bar{c} = 0.8$ are also shown in dotted red lines in Fig. 2, where $\bar{c} = 0.2$ is on the outside and $\bar{c} = 0.8$ is on the inside of $\bar{c} = 0.5$ relative to the centerline, to provide an indication of flame brush thickness; for a given bulk flow velocity, the high-turbulence cases have a significantly thicker flame brush than the low-turbulence cases. The time-averaged velocity field and flame-shape trends for velocity and in-flow turbulence conditions between these extremes follow the same trends as those shown here.

In all cases, the equivalence ratio and temperature of the reactant mixture is held constant and so the laminar flame speed is constant. However, the turbulent flame speed is a function of the inlet turbulence level, and so the location of the flame relative to the shear layer varies for each case. For

9

example, as the bulk flow velocity decreases at a given turbulence intensity, the flame stabilizes at a wider angle as the turbulent flame speed is constant. Furthermore, as the turbulence intensity increases at a given bulk flow velocity, the flame angle widens because the turbulent flame speed increases and the flame can propagate further into the stream.
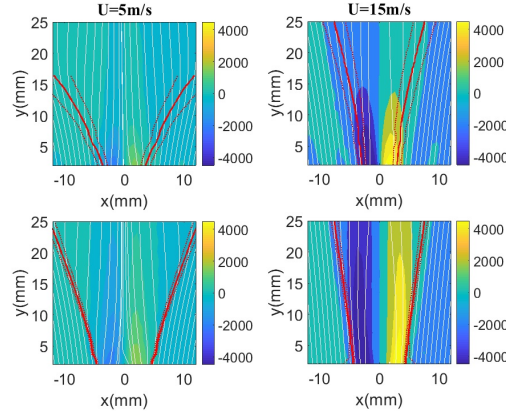

Figure 2: Time-averaged vorticity with streamlines for the high turbulence (top) and low turbulence (bottom) cases at bulk velocities of 5 m/s (left) and 15 m/s (right). The red solid lines mark the $\bar{c} = 0.5$ contour and the dotted lines mark the the $\bar{c} = 0.2$ and the $\bar{c} = 0.8$ contours.

In order to test our hypothesis, we calculate the degree of co-location between the flame and the shear layer to determine whether this system is globally stable or unstable. We select the flame location as corresponding to $\bar{c} = 0.5$, obtained from the binarized Mie-scattering images. The location of the shear layer is identified by calculating the peak time-averaged vorticity at every downstream location. Inspection of the time-averaged flow field and progress variable contours in Fig. 2 shows that in all three cases, the flame becomes taller and moves inward towards the shear layer as the bulk flow

velocity is increased; this is a result of the kinematic condition, where the turbulent flame speed doesn't change significantly but the bulk flow velocity does. It can be seen that for the same bulk flow velocity, the flame moves upstream away from the shear layer as turbulence intensity increases due to the enhancement of turbulent flame speed by the increasing in-flow turbulence. In this way, turbulence has an effect on both the time-averaged and dynamical features of the flow.

This offset between the shear layer and the flame is plotted in Fig. 3 as a single offset metric, following Emerson et al. [16], where δ_ρ is the flame location, δ_ω is the shear layer location, and D is the diameter of the bluff body. The offset is calculated three bluff body diameters downstream of the bluff body and is plotted as a function of bulk flow velocity for three in-flow turbulence conditions. Analysis from Emerson et al. [16], suggests that these offset values correspond to *globally stable wakes* in all cases.
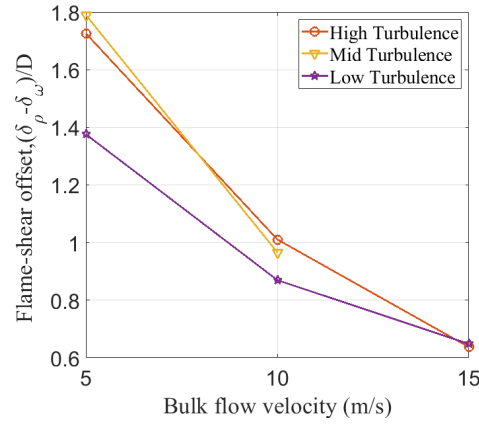

Figure 3: Variation of flame-shear offset with turbulence intensity and bulk flow velocity.

3.2. Time-domain analysis using wavelet transforms

In order to study the evolution coherent dynamics of the flow with increasing turbulence, a time-domain analysis is needed. In this study, we use wavelet transforms to analyse the frequency content of the time-varying signal. Once the coherent oscillations are identified, we use the wavelet transform to identify the frequencies of interest and then reconstruct the selected frequency bands. We use wavelet transforms in this study because, unlike a Fourier transform, wavelet transforms allow for the characterization of the inherently non-stationary signals, such as those seen in flows that experience intermittent coherent oscillations.

To quantify time-varying coherent behavior of the flow field, a time series of the cross-stream velocity is created by averaging the velocity signals in a 6x6 interrogation-window region located at the maximum time-averaged vorticity location of the shear layer for each bulk flow velocity and turbulence intensity condition. Results of the analysis from the cross-stream and axial velocity signals are similar, so only one is presented. The maximum vorticity region is chosen as it represents the region with the most intense vorticity dynamics. The signal is averaged over a region to avoid spurious results that can arise from using a single interrogation window of PIV data. The continuous wavelet transform is done using the *cwt* function in MATLAB and the 'bump' wavelet is used.

Figure 4 shows the magnitude scalograms obtained from the wavelet transforms for the two extreme turbulence intensities and bulk flow velocities shown in Fig. 2. In the 5 m/s, high-turbulence case (top-left of Fig. 4), coherent oscillations can be seen intermittently in frequency ranges between 160 Hz

and 400 Hz, or Strouhal numbers between 0.10 and 0.25. As bulk velocity is increased, the frequency of the coherent oscillations increases, which is to be expected because the characteristic frequency of vortex shedding scales with Reynolds number. For a cylindrical bluff body, the characteristic shedding frequency occurs at a Strouhal number of 0.21 [9], which would correspond to a frequency of 330 Hz at 5 m/s and 990 Hz at 15 m/s. When compared to the high-turbulence cases, the low-turbulence cases have almost no coherent content in the frequency ranges expected for wake vortex dynamics. This indicates that hydrodynamic modes are globally stable and the intermittent coherent oscillation events observed in Fig. 4 at large turbulence intensities are the response of the flow to stochastic forcing by turbulence fluctuations [17, 18].
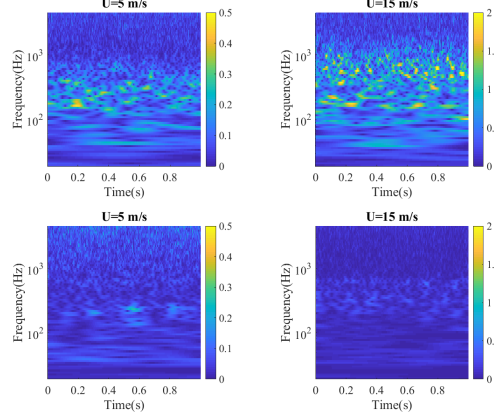

Figure 4: Wavelet transform magnitude scalograms for the high-turbulence (top) and low-turbulence (bottom) cases at bulk velocities of 5 m/s (left) and 15 m/s (right).

13

3.3. Quantification of intermittency in coherent dynamics

The scalograms in Fig. 4 show that the coherent motion at the wake-shedding frequencies occurs intermittently in short bursts. To quantify this intermittency and compare it between cases with different turbulence intensities and bulk flow velocities, we calculate the intermittency factor, following Prasad and Williamson [9], which is equal to the time that the signal is coherent divided by the total time of the signal. To calculate the coherent time for each condition, we first isolate the signal around the high-amplitude frequencies from the wavelet transforms. The spectral widths of the selected signal are kept constant for each bulk flow velocity and increase in width as the velocity increases due to the spectral broadening visible in the high-turbulence cases. The selected spectral bands are as follows: 160-400 Hz for 5 m/s, 240-800 Hz for 10 m/s, and 420-1100 Hz for 15 m/s. Within the selected spectral band, we then choose a local threshold value such that the time periods where the mean signal amplitude across the band exceeds the threshold value are counted as coherent times, represented by τ_c. In this analysis, the threshold chosen was 55% of the peak signal value; however, the trends remain similar for threshold values between 30% and 60%.

Figure 5 shows the dependence of the intermittency factor on bulk flow velocity for the three in-flow turbulence levels. A non-reacting measurement was also analysed at the high-turbulence in-flow condition as a baseline for comparison. In the non-reacting case, increasing the bulk flow velocity reduces the coherent time, resulting in more intermittency in the signal. For the reacting cases, it can be seen that as the in-flow turbulence intensity increases, the coherent time fraction also increases. However, the trend in

14

coherent fraction for the reacting cases is non-monotonic with bulk flow velocity, which is different from the non-reacting case.
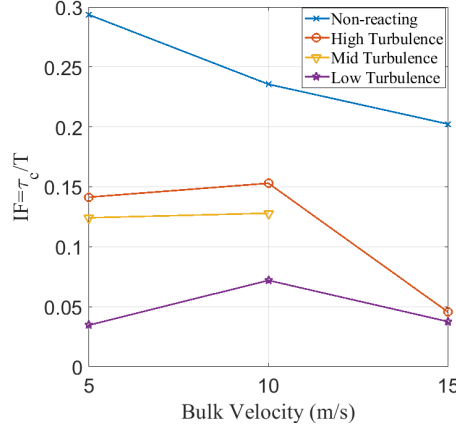

Figure 5: Variation of intermittency factor with bulk flow velocity and in-flow turbulence intensity.

To better interpret the results in Fig. 5, compare the intermittency factor for the high-turbulence intensity 5 m/s case and the low-turbulence intensity 15 m/s case. According to Table 1, these two cases have essentially the same turbulence level: 0.9 m/s for the high-turbulence case and 0.87 m/s for the low-turbulence case. However, the intermittency factors are significantly different; the high-turbulence case displays coherent behavior a factor of three more frequently ($\tau_c = 0.15$) than the low-turbulence case ($\tau_c = 0.05$) despite the same external perturbation level.

These results in intermittency factor match the behavior that would be expected from a globally-stable, noise-driven oscillator. Given that the flow is globally stable, as indicated by the flame/shear offset calculation in Fig. 3, no *self-excited* coherent oscillations are expected from the wake-shedding mode.

As such, high enough in-flow perturbations, like high-intensity turbulence with a wide frequency spectrum, can drive a flow response comprised of contributions from one or more globally stable modes [18]. The mode that dominates the response is the mode that is most effectively forced by the turbulence in the flow regions where it is receptive to forcing [15]. The regions of receptivity depend on the time-averaged mean flow field. As such, these are influenced in the present experiment by both the nominal axial flow velocity, the time-averaged density field, and the offset between the two (flame/shear offset).

This conclusion is different from that of Emerson et al. [16], who showed that turbulence resulted in changes in *flow stability*, not just onset of coherent oscillations. In our case, not only is the system far from the stability boundary, as compared to the Emerson et al. study, as a result of the high density ratio, but also the coherent "bursts" are short duration, encompassing only a few oscillations at a time. If the turbulent fluctuations did indeed cause a change in the global stability, we would expect longer-duration bursts that account for the instability growth and saturation times. As a result, it is much more likely that this flow's behavior is that of a stochastically-forced, globally-stable oscillator.

In particular, the increasing intermittency factor in Fig. 5 suggests that having a larger flame/shear offset increases the receptivity of the mode to a given level of external perturbation. Going back to the comparison of the high-turbulence intensity 5 m/s case and the low-turbulence intensity 15 m/s case, the flame/shear offset for the low-turbulence intensity case is 0.65 compared to an offset of 1.75 for the high-turbulence intensity case. The trends

16

in Fig. 5 show that the corresponding IF is higher for the high-turbulence intensity case, which suggests that the increased flame/shear offset increases the receptivity [4].

3.4. Modal analysis using Proper Orthogonal Decomposition

In this section, we explore the structure of the coherent flow oscillations using proper orthogonal decomposition (POD) [19]. Applying POD directly to the raw velocity signal would not be useful for two reasons. First, the mathematical formulation for the POD is not frequency selective, which can spread coherent frequency content across several modes [20]. Second, the POD is an energy-ordered decomposition based on the total energy of the signal. For non-stationary signals like those in this study, the energy associated with intermittent coherent oscillation events is not significantly larger than that of incoherent motions; applying POD directly on the raw data would not yield modes that are representative of the intermittent coherent oscillations. Therefore, select frequency scales need to be isolated before performing an eigenvalue decomposition such as POD.

To that end, the velocity time series at each point in the flow field is subjected to the wavelet transform and the significant spectral bands are selected, as described in the previous section. We reconstruct the velocity signal associated with the coherent oscillations using a frequency-band-limited inverse wavelet transform in the frequency bands selected. We use the *icwt* function in MATLAB at all points in the flow domain to reconstruct the selected spectral bands. This yields the temporal evolution of the velocity components associated with the intermittent oscillations alone. Proper orthogonal decomposition is performed on this wavelet-filtered time series of

17

velocity in order to extract the flow oscillation mode shapes that correspond to the intermittent coherent oscillation events. This method, similar to the one used by Yin et al.[21], will be referred to as the wavelet-filtered POD (WPOD) in the rest of this paper.

Figure 6 shows the first four WPOD mode shapes of the wavelet-filtered, streamwise component of velocity for the 15 m/s case with the highest in-flow turbulence intensity. Two distinctive mode shapes can be observed: sinuous or anti-symmetric (modes 1 and 2) and varicose or symmetric (modes 3 and 4) motions. Similar results are found for all cases, where among the highest-energy modes of the WPOD, both symmetric and anti-symmetric motions are observed. Our analysis shows that in all the high-turbulence intensity cases for all bulk-flow velocities, the dominant mode pairs exhibit sinuous motion.
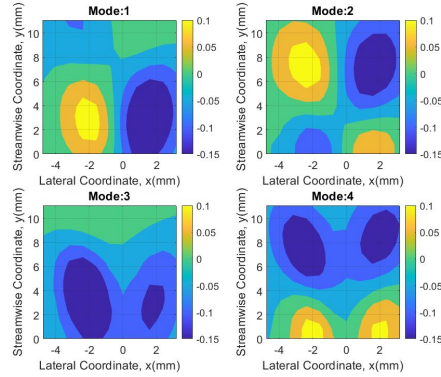

Figure 6: First four streamwise WPOD mode shapes for case with high-turbulence intensity and bulk flow velocity of 15 m/s.

In the low-turbulence intensity cases, the mode shapes vary more significantly based on flow velocity. Figure 7 and Fig. 8 show the first two modes
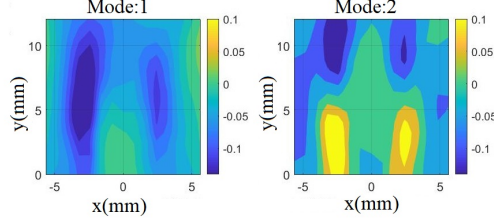
Figure 7: First two WPOD modes for the streamwise velocity for the 10 m/s flow with low turbulence intensity.
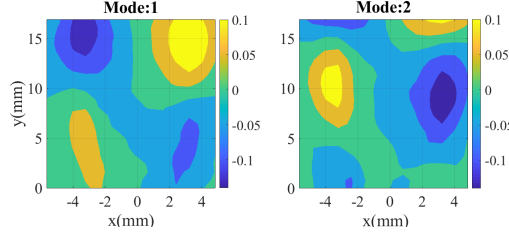

Figure 8: First two WPOD modes for the streamwise velocity for the 15 m/s flow with low turbulence intensity.

of the low-turbulence intensity cases for 10 m/s and 15 m/s bulk velocities, respectively. In the 10 m/s case, the dominant mode shape is symmetric, or varicose, but the overall energy contribution of these modes is low compared to other cases; this energy is quantified further next. Additionally, the mode shape does not have as coherent and distinctive a structure as the high-turbulence intensity cases and the velocity time-series reconstructions of these modes show significant intermittency in the vortex shedding patterns. At 15 m/s (Fig. 8), however, the sinuous shedding pattern is again seen in the first two modes, showing more similarities to the higher in-flow turbulence cases.

The WPOD analysis suggests that when the flow oscillations are coher-

19

ent, the wake oscillates in a sinuous manner. In order to quantify the level of coherent sinuous motion captured by the filtered wavelet transforms, we decomposed the wavelet-filtered time series of the coherent time periods into their sinuous and varicose contributions, following the work of Emerson et al. [4]. The purpose of this decomposition is to identify how much of the 'coherent time', τ_c, is governed by the sinuous and varicose motions and also to characterize the strengths of the two types of oscillations. Equation 1 describes the decomposition of vorticity into sinuous and varicose components. In each of these equations, the vorticity on either side of the flow centerline ($\omega(x,t)$ and $\omega(-x,t)$) is compared to determine the relative phase between the two sides; if the two sides oscillate in-phase, then the motion is sinuous and if they oscillate out-of-phase, then the motion is varicose.

$$
\begin{aligned}
\omega_{sinuous}(x,t) &= \frac{\omega(x,t) - \omega(-x,t)}{2} \\
\omega_{varicose}(x,t) &= \frac{\omega(x,t) + \omega(-x,t)}{2}
\end{aligned}
\tag{1}
$$

These components are converted to time-domain 'energy-like' terms using the relations in Eqn. 2.

$$
\begin{aligned}
e_s(t) &= \int_0^W \omega_{sinuous}^2 \, dx \\
e_v(t) &= \int_0^W \omega_{varicose}^2 \, dx
\end{aligned}
\tag{2}
$$

By calculating the percentage of sinuous and varicose energy content at each time, we see that nearly all the time frames ($\geq 98\%$ of time frames) corresponding to coherent motion are predominantly sinuous ($\geq 50\%$ sinuous energy).
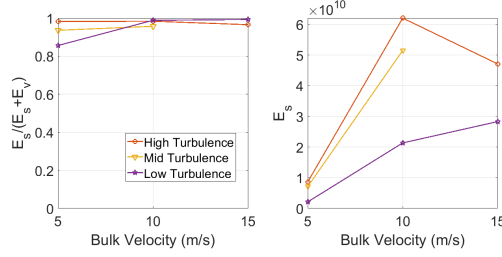
20

Figure 9: Variation of time integrated sinuous energy fraction as a function of bulk flow velocity and in-flow turbulence

Figure 9 shows the time-integrated sinuous energy fraction and the absolute time integrated sinuous energy (E_s and E_v) for different turbulence intensities. E_s and E_v were obtained by integrating e_s and e_v from equation 2 in time over all the coherent frames. It can be seen, in all cases analysed, that almost all ($\geq 85\%$) of the energy corresponding to the intermittent oscillation events is sinuous, which is evidence that the dominant mode is the sinuous vortex shedding mode, as seen in the WPOD analysis.

The absolute time-integrated sinuous energy varies significantly with turbulence intensity, where the low-turbulence cases have a lower sinuous energy; this is also similar to the results seen in the POD in Figs. 7 and 8. Figure 9 illustrates a key point of this study: the interplay between receptivity of the sinuous mode and the amplitude of stochastic forcing required to excite the sinuous mode. In cases where the receptivity is high (due to high flame/shear offset), low forcing amplitudes still result in a sinuous mode, and in the cases where receptivity is low, high forcing amplitudes are required to see a strong sinuous mode.

This symmetry decomposition result, like the WPOD analysis, shows that the flow exhibits a noise-driven, globally-stable wake mode, and that

21

the receptivity of this mode to external perturbations is a function of the degree of spatial separation between the flame and the shear layer.

4. Conclusions

This study focuses on understanding and quantifying the interaction between stochastic fluctuations and coherent structures present in rod-stabilized flames. High-speed stereoscopic PIV was used to obtain the velocity fields and flame edges for a rectangular burner with a rod-stabilized flame. Three in-flow turbulence intensities and three bulk-flow velocities were studied. The key contribution of this work is the characterizing the response of the flow to the stochastic forcing amplitude (turbulence intensity) and location of the flame with respect to the shear layer.

Intermittency of the coherent motion is quantified using wavelet transforms, an intermittency factor and the flow oscillation mode shapes associated with intermittently occurring coherent oscillation events which are extracted using a wavelet-filtered POD method. These methods show that the dominant coherent oscillation is sinuous wake oscillation. This result was further confirmed from symmetry decomposition of the reconstructed time-filtered data. It is seen that the coherent motion becomes more frequent and continuous with increasing in-flow turbulence as a result of stochastic forcing of the marginally-stable system appears to be the driving mechanism for wake oscillation. This work highlights the impact that turbulence has on different oscillation modes that govern the dynamics of a bluff-body stabilized flame and the insight obtained about these interactions could be applied to more complex configurations. The role of the turbulence is two-fold, as it controls

not just the amplitude of the stochastic forcing, but also the turbulent flame speed and hence the flame/shear offset as well; this coupled dependence of the system response on turbulence can be seen in the non-monotonic behavior of the intermittency factor in Fig. 5.

This result has implications for both the static and dynamic stability of lean-premixed combustion systems. Velocity-coupled thermoacoustic oscillations require the presence of coherent velocity fluctuations to drive flame area fluctuations [22]. If the noise-driven oscillations occur at frequencies close to the acoustic resonant frequency of the system and the bursts of coherent motion driven by the turbulent oscillations are of high enough amplitude and long enough duration, thermoacoustic instability could arise [23]. Further understanding of the role of turbulence in the coherent dynamics of combustion systems can help in avoiding these detrimental operability issues.

Acknowledgments

References

[1] T. Lieuwen, Unsteady combustor physics, Cambridge University Press, 2012.

[2] S. Chaudhuri, S. Kostka, M. W. Renfro, B. M. Cetegen, Blowoff dynam-

ics of bluff body stabilized turbulent premixed flames, Combustion and Flame 157 (4) (2010) 790–802.

[3] R. Erickson, M. Soteriou, The influence of reactant temperature on the dynamics of bluff body stabilized premixed flames, Combustion and Flame 158 (12) (2011) 2441–2457.

[4] B. Emerson, J. O'Connor, M. Juniper, T. Lieuwen, Density ratio effects on reacting bluff-body flow field characteristics, Journal of Fluid Mechanics 706 (2012) 219–250.

[5] D. Durox, T. Schuller, S. Candel, Combustion dynamics of inverted conical flames, Proceedings of the Combustion Institute 30 (2) (2005) 1717–1724.

[6] S. J. Shanbhogue, M. Seelhorst, T. Lieuwen, Vortex phase-jitter in acoustically excited bluff body flames, International Journal of Spray and Combustion Dynamics 1 (3) (2009) 365–387.

[7] A. Karmarkar, M. Frederick, S. Clees, D. Mason, J. O'Connor, Role of turbulence in precessing vortex core dynamics, in: ASME Turbo Expo, 2019.

[8] S. Kheirkhah, Ö. Gülder, Topology and brush thickness of turbulent premixed v-shaped flames, Flow, Turbulence and Combustion 93 (3) (2014) 439–459.

[9] A. Prasad, C. H. Williamson, The instability of the shear layer separating from a bluff body, Journal of Fluid Mechanics 333 (1997) 375–402.

[10] V. Nair, G. Thampi, R. Sujith, Intermittency route to thermoacoustic instability in turbulent combustors, Journal of Fluid Mechanics 756 (2014) 470–487.

[11] B. R. Chowdhury, B. M. Cetegen, Experimental study of the effects of free stream turbulence on characteristics and flame structure of bluff-body stabilized conical lean premixed flames, Combustion and Flame 178 (2017) 311–328.

[12] S. Nair, T. Lieuwen, Near-blowoff dynamics of a bluff-body stabilized flame, Journal of Propulsion and Power 23 (2) (2007) 421–427.

[13] B. R. Chowdhury, B. M. Cetegen, Effects of free stream flow turbulence on blowoff characteristics of bluff-body stabilized premixed flames, Combustion and Flame 190 (2018) 302–316.

[14] A. Tyagi, I. Boxx, S. Peluso, J. O'Connor, Statistics and topology of local flame–flame interactions in turbulent flames, Combustion and Flame 203 (2019) 92–104.

[15] F. Giannetti, P. Luchini, Structural sensitivity of the first instability of the cylinder wake, Journal of Fluid Mechanics 581 (2007) 167—197.

[16] B. Emerson, D. Noble, T. Lieuwen, Stability analysis of reacting wakes: The physical role of flame-shear layer offset, in: AIAA SciTech Forum, 2014.

[17] J. Fontane, P. Brancher, D. Fabre, Stochastic forcing of the lamb–oseen vortex, Journal of Fluid Mechanics 613 (2008) 233–254.

[18] B. F. Farrell, P. J. Ioannou, Stochastic forcing of the linearized navier–stokes equations, Physics of Fluids A: Fluid Dynamics 5 (11) (1993) 2600–2609.

[19] G. Berkooz, P. Holmes, J. L. Lumley, The proper orthogonal decomposition in the analysis of turbulent flows, Annual Review of Fluid Mechanics 25 (1) (1993) 539–575.

[20] A. Towne, O. T. Schmidt, T. Colonius, Spectral proper orthogonal decomposition and its relationship to dynamic mode decomposition and resolvent analysis, Journal of Fluid Mechanics 847 (2018) 821–867.

[21] Z. Yin, M. Stöhr, Time–frequency localisation of intermittent dynamics in a bistable turbulent swirl flame, Journal of Fluid Mechanics 882 (2020).

[22] C. O. Paschereit, E. Gutmark, W. Weisenstein, Excitation of thermoacoustic instabilities by interaction of acoustics and unstable swirling flow, AIAA Journal 38 (6) (2000) 1025–1034.

[23] S. Hemchandra, S. Shanbhogue, S. Hong, A. F. Ghoniem, Role of hydrodynamic shear layer stability in driving combustion instability in a premixed propane-air backward-facing step combustor, Physical Review Fluids 3 (6) (2018) 063201.